physica status solidi a

phys. stat. sol. (a) **204**, No. 6, 1712–1720 (2007) / **DOI** 10.1002/pssa.200675362

Structural and transport properties of Nb nanowires

Zhenting Dai, Chun Zhang, Robert N. Barnett, Alexei Marchenkov*, and **Uzi Landman****

School of Physics, Georgia Institute of Technology, Atlanta, GA 30332-0430, USA

Received 31 October 2006, accepted 3 January 2007
Published online 23 May 2007

PACS 68.65.La, 73.40.Jn, 73.63.Rt, 74.45.+c

High-resolution conductance measurements in niobium nanowires below the superconducting transition temperature are presented. Results are shown for a complete multistage elongation-compression cycle of a nanoscale contact. We focus on a bistability region which manifests itself as random telegraph noise. Density functional structural optimizations and conductance calculations using the non-equilibrium Green's functions method reproduce and explain the measurements. In particular, the observed bistability is associated with formation of a niobium dimer between the opposing electrodes, with the dimer shuttling between a symmetric, high conductance, and an asymmetric, low conductance, configurations in the gap.

1 Introduction

Formation of nanowires (NWs) suspended between a tip and a surface was discovered through early molecular dynamics simulations [1] which were aimed at exploring contact formation, nanoindentation, the atomic origins of frictional processes and tip-substrate interactions [1–5]. Subsequent research efforts pertaining to the structural, mechanical, electrical, and chemical properties of nanowires, continue to be an active area of scientific endeavor [6–16]. These early simulations have shown formation of a nanowire junction, generated, at room temperature, in the course of an adiabatically slow separation of a nanocontact between a tip and a surface (nickel tip and gold surface in the original work [1]). Nanowires formed in this manner (or via adiabatic elongation of a contact in general, for example through the use of a mechanically controlled break junction [6, 11]) were found in the simulations to exhibit highly ordered crystalline structures. These nanowires are predicted to possess nearly ideal mechanical properties (that is, enhanced critically resolved axial stresses that are much higher than those of the bulk metal [1, 8, 9]) reflecting the defect intolerance of nanoscale structures, their high annealing propensity resulting from a very large surface-to-volume ratio that is characteristic to nanoscale systems, and their dislocation-less mechanical deformation mechanisms.

The contact elongation process was found to proceed through a sequence of structural instabilities, each comprised of stress accumulation and yield stages (with the elongation process localized to the neck region of the junction). These structural evolution patterns have been shown through the simulations [1] to be portrayed in oscillations of the force required to elongate the wire, with a period approximately equal to the interlayer spacing. The saw-tooth character of the predicted force oscillations reflects the stress accumulation and relief stages of the elongation mechanism.

These predictions, as well as anticipated electronic conductance properties [that is, point contact characteristics and conductance quantization in units of the conductance quantum ($G_0 = 2e^2/h$, $G_0^{-1} = 12.9\ \mathrm{k}\Omega$)], have been corroborated in a number of experiments using scanning tunneling and force

* Corresponding author: e-mail: alexei.marchenkov@physics.gatech.edu, Phone: +1 404 385 0875, Fax: +1 404 894 9958
** e-mail: uzi.landman@physics.gatech.edu

microscopy [6, 7, 9, 12–15], break junctions [6, 11], and pin-plate techniques [8] at ambient environments, as well as under ultrahigh vacuum and/or cryogenic conditions. Particularly interesting are experimental (room temperature) observations [9] of the oscillatory behavior of the elongation forces and of direct correlations between the step-wise changes in the conductance and the force oscillations (portraying the predicted structural evolution) [16], as well as theoretical and experimental observations of mechanical and structural reversibility in elongation-compression cycles of nanowires that are reflected also in measured and calculated conductance traces [8]. The conductance quantization in nanowires is in-accord with the Landauer theory [17, 18] where the total conductance is given by $G = G_0 \sum_{j=1}^{N} \tau_j$ with $\{\tau_j\} \equiv \{\tau_1, \ldots, \tau_N\}$ denoting the set of transmission coefficients of the N channels that contribute to the NW conductance at a given NW configuration. The channel composition $\{\tau_j\}$ can be deduced from low-voltage $I-V$ characteristics of atomic-size superconducting point contacts or NWs [19–22].

One of the most fascinating aspects of nanowires is the prospect of formation of atomic-scale contacts and switches [1, 14, 23–27], which may occur towards the ultimate stages of elongation (that is before complete physical separation, or breaking, of the wire). Such atomically thin nanowires have indeed been observed in the aforementioned early simulations of gold nanowires [1]. More recently gold nanowires have been imaged by high-resolution transmission electron microscopy (HRTEM) as a gold STM tip was retracted from a gold surface [28], confirming the early theoretical predictions. Moreover, gold dimers suspended in the gap between the tips of two opposing electrodes have been predicted through first-principles molecular dynamics simulations [29]; in this study it was shown that elongation leads eventually to breakup of the dimer with one of the atoms bonding to one of the electrodes and the second one adhering to the the other electrode. Formation of atomic gold chains comprised of several atoms has also been reported in break-junction experiments [30], and imaged via HRTEM as connecting bridges between areas in thin gold films perforated by impact of energetic electrons [28, 31].

As aforementioned, it has been predicted theoretically and shown experimentally that the structural and transport properties of NWs are correlated to each other. In particular, adjusting a contact precisely at conductance jumps between neighboring plateaus may lead to fluctuations between two discrete values in the form of random telegraph noise (RTN), involving high and low conductance states (HG and

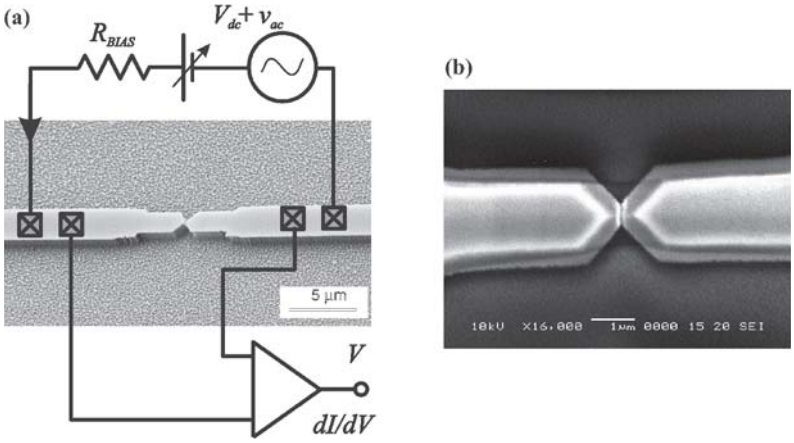

Fig. 1 (a) Scanning electron micrograph of a niobium microfabricated mechanically controlled break junction. A diagram of the measurement setup is superimposed. (b) Magnified top view of one of the junctions taken after a breaking experiment. Unlike tensile materials, such as gold or aluminum, which show substantial plastic deformations in the contact region, our niobium samples appear to break along two microcrystalline facets. The horizontal bar at the middle bottom of panel (b) corresponds to a length of 1 μm.

LG, respectively), whose origin remains unknown [11, 32]. However, short of direct imaging of the NW structure during elongation and simultaneous measurement of the conductance [28], evidence for the aforementioned close correlation between the structural and transport characteristics is lacking.

Here we report on experimental and theoretical studies of niobium contacts in the final stages before breakup, when the conductance is of the order of $2-4G_0$ with a few contributing channels. We present experiments performed on microfabricated mechanically-controlled break junctions (MCBJ) in a cryogenic setup that permits very high levels of stability and control over the elongation process. Analysis of data obtained during reversible manipulation of the contacts below [19, 21, 22a] and above the superconducting transition temperature, allowed determination of the conductance channel compositions at various stages of the elongation process, including a switching stage where two-level RTN is observed. The use of density functional theory (DFT) electronic structure calculations, coupled with structural optimizations and evaluations of the electric conductance (using the non-equilibrium Green's function (NEGF) method [33, 34]) allowed us to determine that the NW structure underlying, and consistent with, the complete set of experimental observations, consists of a Nb dimer suspended between the two electrodes. The calculated conductance variations as a function of elongation, reversibility, patterns revealed in the channel composition, and two-level switching behavior between HG and LG states corresponding to symmetric and asymmetric positions of the dimer in the gap (with the latter one predominating for larger gap widths), faithfully reproduce the experimental observations [22b].

2 Methods

As aforementioned, we used microfabricated samples in a cryogenic MCBJ set-up (see Fig. 1) prepared by dc-magnetron sputtering of Nb onto a 1 μm thick insulating polyimide layer covering a flexible bronze substrate [22a]. The film deposition was performed in the presence of a liquid-nitrogen shield to avoid deterioration of the superconducting properties of niobium by outgasing of water, polyimide and the organic photoresist (PMMA) mask. The width, thickness, and length of the suspended constrictions were all ~100 nm. The procedure was optimized for producing high superconducting transition temperatures, which tends to yield microcrystalline thin films [35]. SEM micrographs of samples previously used in our experiments indicate that breaking occurs by cleaving along the boundary between two microcrystallites (see Fig. 1(b)). Our MCBJ set-up yields remarkably stable contacts and allows reversible manipulation of the electronic structure of the contact within ~1 Å elongation range. We could restore the length of the contact with an accuracy better than 1 pm and reproduce highly nonlinear $I-V$ and conductance ($\mathrm{d}I/\mathrm{d}V$) characteristics, even after several hours of experimentation. All measurements reported here were performed in ultra-high vacuum conditions at 4.2 and 9 K.

Insights into the nature of bonding, atomic arrangements, structural transitions and electronic transport in Nb nanowires formed upon the separation of the leads were obtained through density functional theory (DFT) electronic structure calculations [36] and conductance calculations with the combination of DFT and the non-equilibrium Green's function method (NEGF) [33, 34, 37]. The DFT calculations include the generalized gradient approximation, GGA [38], using a plane wave basis (kinetic energy cutoff $E_{\mathrm{cut}} = 68$ Ry), and norm-conserving soft pseudopotentials [39]. In the pseudopotential construction we used as a reference configuration [Kr] $4s^2 4p^6 4d^5 5s^0$, i.e. 13 valence electrons per atoms as described in Ref. [40]. In this scheme the electronic configuration of the atom is given correctly to be [Kr] $4s^2 4p^6 4d^4 5s^1$.

3 Results

We begin by describing a full elongation-compression cycle of the nanowire contact that started at a configuration having a conductance of ~$4.4G_0$, see Fig. 2. Upon elongation of the contact by 0.4 Å (interval AB), a sudden jump occurred (BC), indicating switching of the contact into another configuration (interval CD). This interval contains a region of slow two-level random telegraph noise (RTN) flanked by high (HG) and low (LG) conductance branches. For this particular contact realization the difference in

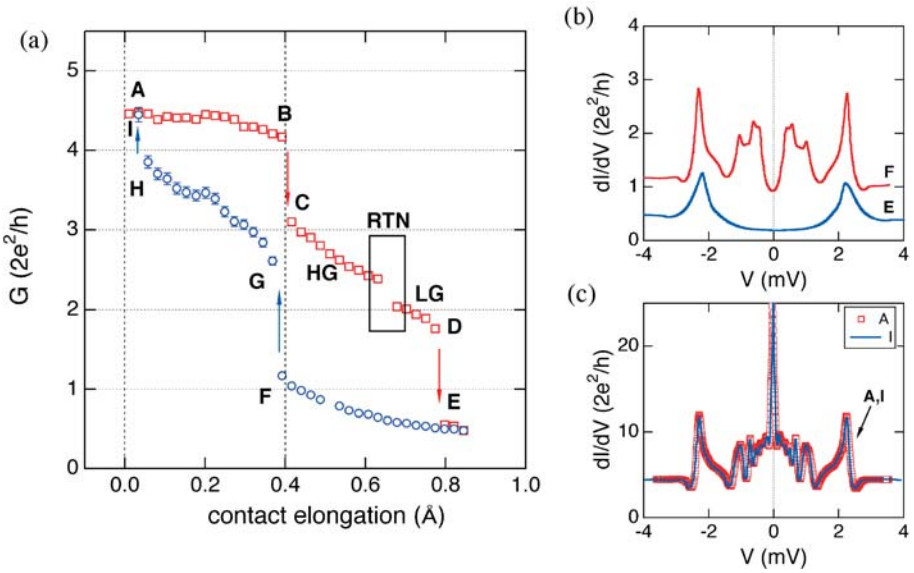

Fig. 2 (online colour at: www.pss-a.com) (a) Elongation–compression cycle of a Nb contact at 4.2 K. Squares (red online) represent stretching of the contact and formation of the nanowire; circles (blue online) correspond to compression. In this contact configuration, the initial conductance was ~4.4G_0. After elongating the nanowire by 0.4 Å (interval AB), a sudden jump occurred (BC), indicating switching of the contact into another configuration (interval CD). This interval contains a region of slow two-level random telegraph noise (RTN) flanked by high (HG) and low (LG) conductance branches. After elongating the NW by 0.8 Å from the initial configuration (point D), the contact switched abruptly into a tunnel junction (E), as evidenced by the exponential dependence of the conductance on the elongation during the nanowire compression (interval EF), as well as from the conductance spectra (dI/dV vs. V) shown in panel (b), where we display data corresponding to points E and F (see panel (a)). The compression of the tunnel junction culminates in a sudden jump to contact (F to G) at nearly the same electrode separation as the B to C step during the stretching. The resulting configuration was further compressed up to a conductance of ~3.8G_0 (H), where it abruptly switched into configuration I. This last configuration was found to be identical to the one at the beginning of the cycle (A). To demonstrate this finding we show in panel (c) the conductance spectra for configurations A and I. The total time interval between the measurements of the spectra at A and I was 12 hours.

conductance between the HG and LG states in the RTN region is ~0.3G_0. This value is smaller than the more often occurring one of ~0.5G_0 (see below). Subsequent elongation of the NW by 0.8 Å from the initial configuration (point D), causes the contact to switch abruptly into a tunnel junction (E), as evidenced by the exponential dependence of the conductance on the elongation during the nanowire compression (interval EF), as well as from the conductance spectra (dI/dV vs. V) shown in panel (b), where we display data corresponding to points E and F (see panel (a)). Here we note low values of differential conductance at a vanishing bias voltage. The compression of the tunnel junction culminates in a sudden jump to contact (F to G), that occurred at nearly the same electrode separation as the B to C step during the stretching. The resulting configuration was further compressed up to a conductance of ~3.8G_0 (H), where it abruptly switched into configuration I. This last configuration was found to be identical to the one at the beginning of the cycle (A). To demonstrate this finding we show in panel (c) the conductance spectra for configurations A and I. The total time interval between the measurements of the spectra at A and I was 12 hours.

In what follows, we focus on investigations pertaining particularly to the random telegraph noise region and the high and low conductance branches adjacent to it. For this purpose we display results corresponding to measurements with a larger difference between the HG and LG branches, i.e. 0.55G_0, see

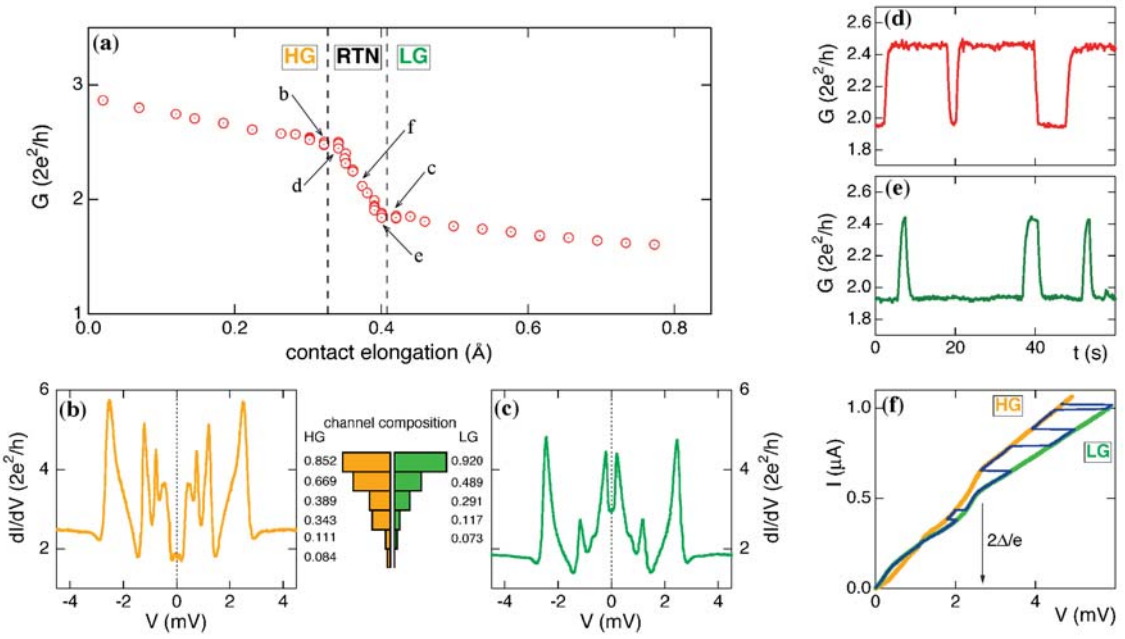

Fig. 3 (online colour at: www.pss-a.com) (a) Reversible variation of the conductance versus elongation distance recorded at 4.2 K. Similar results were obtained above the superconducting transition temperature. With further elongation the NW breaks. (b), (c) The differential conductance of the HG (b, yellow online) and the LG (c, green online) states versus voltage measured at 4.2 K. The measurements correspond to points b and c in panel (a). The corresponding channel compositions are shown in the inset between (b) and (c). (d), (e) Temporal conductance fluctuations near the HG and LG states, respectively, taken at points d and e in panel (a). The contacts were current-biased at $I_{\text{bias}} = 0.75\,\mu\text{A}$. (f) Switching between the two states recorded while acquiring the $I-V$ characteristics in the middle of the RTN region (solid line, blue online). The curves marked HG and LG (yellow and green online) correspond to the dI/dV curves shown in (b) and (c). The acquisition of each curve in (f) takes about two minutes.

Fig. 3(a). In this measurement we started by adjusting the contact's conductance to just below ~$3G_0$ using a coarse screw actuator. This conductance corresponds to the most probable atomic configuration as can be judged from the conductance histogram obtained using notched-wire samples [21]. From this point, we used the fine piezo actuator. After adjusting the length, we measured the contact's current–voltage ($I-V$) and conductance (dI/dV) characteristics and determined the channel composition. Typical behavior seen in 18 contact realizations from 5 different samples is as follows: as the contact was stretched, the conductance gradually decreased to $2.4 \pm 0.15G_0$ (Fig. 3(a)); subsequently, in an elongation range of ~0.1 Å we observed slow two-level fluctuations (with a conductance difference of up to $0.6G_0$) between well defined HG and LG values, which showed characteristics of RTN (Fig. 3(d)–(f)); upon further elongation, the state with lower conductance was stabilized (Fig. 3(a), (e)). At any point, the direction of the contact length adjustment could be reversed and the conductance behavior reproduced without detectable hysteresis. Elongation beyond the range shown in Fig. 3(a) results in breakup of the contact.

The conductance evolution curve shown in Fig. 3(a) includes multiple traversing of the RTN region, where the conductance was obtained by time-averaging of the two-level fluctuations (Fig. 3(d), (e)). This behavior was reproduced both in the superconducting state, where the conductance is determined from dI/dV on the resistive branch ($eV > 2\Delta$, where Δ is the superconducting gap), and in the normal state at temperatures above our devices' superconducting transition temperature of ~8.8 K. It has been previously shown that suppression of superconductivity in aluminum atomic-size contacts by either raising the

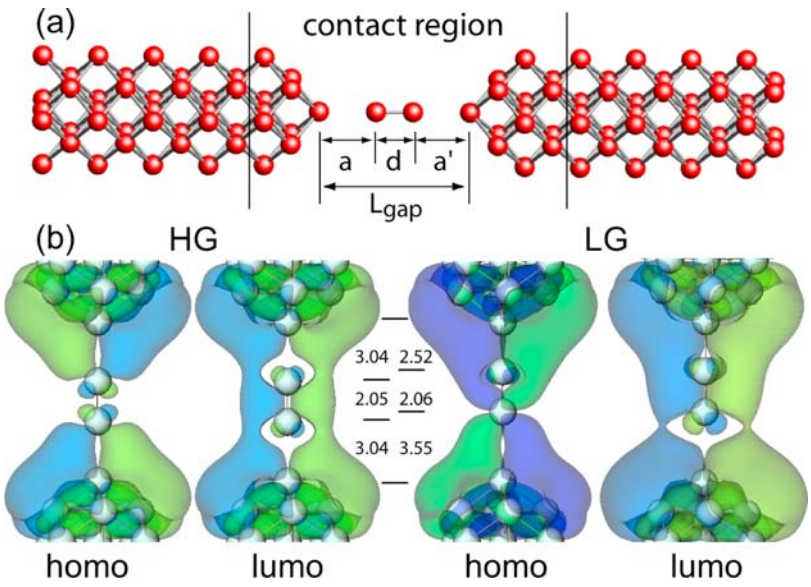

Fig. 4 (online colour at: www.pss-a.com) Nb nanowire configurations and wave functions. (a) The division of the system into the contact region and the two leads. A symmetric Nb dimer is shown in the gap (i.e. $a = a'$). (b) A symmetric high-conductance (HG) configuration (left) and an asymmetric low-conductance (LG) one, both corresponding to $L_{\text{gap}} = 8.13$ Å. For both we show superimposed on the atomic structure iso-surfaces of the highest (lowest) occupied (unoccupied) molecular orbitals, homo (lumo) respectively, with energies close to the Fermi level. The orbitals shown have large overlaps with the conductance eigen-channels. These Kohn–Sham wave functions are made predominantly of d-states and they extend over the Nb dimer and the leads. The two shades (blue and green online) correspond to positive and negative signs of the wavefunctions.

temperature or applying a magnetic field does not affect their electronic structure seen through the channel composition [41]. We have experimentally verified the temperature independence of our results for both the HG and LG states. Differential conductance curves of the HG and LG configurations taken in the vicinity of the RTN region are shown in Fig. 3(b)–(c); the corresponding $I-V$ curves are shown in Fig. 3(f). The most noticeable difference is that there are two high-transparency ($\tau_j \geq 0.6$) channels in the HG state, while there is a single such channel in the LG state (see the inset in Fig. 3); for all experimental contact realizations it is the transparency of the latter channel that was higher than that of the highest-transparency channel of the HG state. This can be qualitatively seen from the higher conductance in the LG state near zero voltage bias (compare Fig. 3(b) and (c)).

Manipulation of the contact length in the RTN region allowed us to change the ratio of the time the NW spent in the two states (Fig. 3(d)–(f)), which is consistent with adjusting the two minima in the double-well potential describing the fluctuating system [42, 43].

We explored first the electronic and atomic structures of several atomic contacts and nanowire configurations spanning the gap between two opposing Nb electrodes of pyramidal shapes (Fig. 4). In structural optimizations all the Nb atoms included in the "contact region" (see Fig. 4(a)) are fully relaxed, while the other atoms (considered as part of the leads) are held in their bulk Nb lattice positions; we have found that changes in the distance between the electrodes express themselves essentially entirely in variations of distances in the gap region only. These relaxed local structures are subsequently used in the NEGF transport calculations which employ semi-infinite bcc (100) leads (consisting of bcc stacked alternating 4- and 5-atom layers) and the contact region (see Fig. 4(a)). In the NEGF calculations we used an atomic basis with the same 10 orbitals per atom as those used in the construction of the pseudopotential, which are then expanded in a plane wave basis with $E_{\text{cut}} = 68$ Ry.

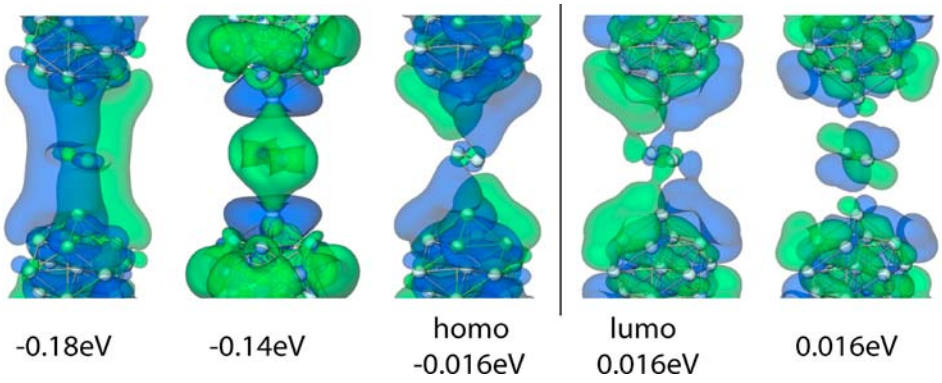

Fig. 5 (online colour at: www.pss-a.com) A configuration of the Nb nanowire corresponding to $L_{gap} = 6.63$ Å with superimposed isosurfaces of the highest (lowest) occupied (unoccupied) molecular orbitals, homo (lumo) respectively, as well as several other orbitals with energies close to the Fermi level: see energy values for each orbital with reference to $E_F = 0$. The Fermi level lies between the homo and the lumo orbitals. In the configuration shown here the axis of the suspended Nb dimer makes an angle of 94 degrees with the *z*-axis (the line connecting the two tip atoms of the electrodes). The other geometric parameters are: the distance between the two Nb atoms in the gap $d = 2.15$ Å and the distance between a Nb atom of the dimer and the nearest Nb tip atom is 3.42 Å. The conductance of this configuration is $3.5G_0$. Note the d-character of the orbitals and their extended nature.

Several configuration that we have explored initially yielded results that do not correspond to the experimental findings: most importantly, they do not show two-level behavior upon stretching of the contact. These include: (i) the case of two electrodes sharing a common vertex atom (separated by the bulk nearest-neighbor distance, $d_{nn} = 2.66$ Å from the nearest atom in the underlying layer) yielding a conductance of ~$5G_0$ [44], and (ii) a configuration where the two electrode tips are bridged by a single suspended atom separated by d_{nn} from each of the tip atoms, with a conductance of $4.8G_0$. As we describe below, the only nanowire configuration whose transport and structural characteristics agree well with the measurements for the entire range of tip-to-tip gap distances, L_{gap}, discussed in this paper, consists of a dimer of Nb atoms suspended in the gap between the opposing Nb electrodes (Fig. 4).

We begin with a gap-width $L_{gap} = 7.6$ Å, where in equilibrium the two Nb nanowire atoms are separated by $d = 2.05$ Å, and their distances from the tip atoms $a = a' = 2.77$ Å. The calculated conductance for this configuration is $3.0G_0$, with a channel composition {0.92, 0.82, 0.48, 0.33, 0.24, 0.1}; we list only channels with $\tau_j \geq 0.1$. This correlates well with the highest measured conductance value shown in Fig. 3. As long as $L_{gap} < 8.0$ Å only a symmetric (i.e. $a = a'$, see Fig. 4(b) left) dimer configuration is found to be stable, with the conductance decreasing slowly and monotonically upon stretching of the contact. However, when $L_{gap} = 8.13$ Å two states of the suspended Nb dimer are found: the lower energy one corresponds to a symmetric dimer, and the higher energy (by 0.4 eV) metastable isomer is a displaced asymmetric dimer configuration (i.e. $a' > a$, see Fig. 4(b) right). The symmetric dimer structure with $d = 2.05$ Å, and $a = a' = 3.04$ Å is an HG state, $G = 2.6G_0$ and a channel composition {0.90, 0.81, 0.39, 0.16, 0.13}, and the asymmetric configuration (LG state) is a local energy minimum in the gap with $d = 2.05$ Å, $a = 2.52$ Å and $a' = 3.57$ Å, and it exhibits a lower conductance ($2.1G_0$) and a corresponding channel composition {0.91, 0.57, 0.30, 0.16, 0.12}. It is noteworthy that the close top two conductance channels ($0.90G_0$ and $0.81G_0$) in the symmetric HG dimer configuration, are split in the asymmetric LG isomeric, with the conductance being dominated by a single channel ($0.91G_0$); a similar trend is seen in the channel composition of the HG and LG states in the RTN region of the measurements (see inset between panels (b) and (c) in Fig. 3). Two-level behavior is also found for an additional (short) stretching range (with a smaller energy difference between the two states).

Throughout the elongation process described above the structural variations of the NW and of the transport characteristics are reversible. However, past a certain elongation the two-state characteristic

behavior ceases, and only a single low conductance state is found, corresponding to an asymmetric dimer. Continued stretching leads to breaking of the NW with the dimer remaining attached to one of the electrodes.

In Fig. 4(b) we display for the HG (symmetric dimer state, $G = 2.6G_0$) and LG (asymmetric dimer state, $G = 2.1G_0$) configurations of the Nb dimer, isosurfaces of wave functions (with energies near the Fermi energy) that are found to have large overlaps with the conductance eigenchannels [45]. The figure provides visualization of the molecular orbitals contributing to electron transport through the NW. The d-character of the orbitals is evident, as well as their extended nature that connects the suspended NW atoms in the gap to the supporting electrodes and leads.

Before closing, we comment on the results of calculations starting with the initial configuration with $L_{gap} = 7.6$ Å, where instead of stretching the contact we compressed it to a value of $L_{gap} = 6.63$ Å. For this compressed configuration we find that in equilibrium the suspended dimer is tilted with its axis forming an angle of 94 degrees with respect to the axis joining the two tip atoms of the opposing electrodes (see Fig. 5 where we show the atomic configuration of the contact region along with iso-surfaces of the wavefunctions near the Fermi level exhibiting *d*-character and extended nature). For this configuration, the calculated conductance is $3.5G_0$. It would be of interest to explore experimentally compression of the contact along the (reversible) interval CD (see Fig. 2(a)), going beyond point C. Such experiments are underway.

4 Summary

We have presented here transport measurements on microfabricated Nb break junctions, that include a complete elongation-compression cycle (Fig. 2) and a detailed investigation of an elongation interval showing reversible evolution from $G \approx 3G_0$ to $G \leq 2G_0$. This reversible region includes a narrow bistability interval where temporal fluctuations between high and low conductance states occur (Fig. 3). Measurements in the superconducting state allowed determination of the channel composition as a function of the degree of elongation, revealing a change in the characteristics of the dominant conducting channels between the two states.

These results are reproduced and explained by DFT calculations and structural optimizations coupled with conductance evaluations. In particular, we conclude that the nanowire consists of a Nb dimer suspended between atomically sharp contacts. The two-level telegraph noise characteristics originate from shuttling of the dimer between a symmetric (high conductance) and asymmetric (low conductance) configurations (Fig. 4). In this manner, we have demonstrated that accurate nanowire manipulations and high resolution conductance measurements, in conjunction with high level theoretical simulations, can serve as a reliable electronic transport spectroscopy and an atomic structure microscopy of nanowires and point contacts [22b].

Acknowledgements We thank Vitaly Shumeiko and Åke Ingerman for their simulation code of transport curves [19] used in the analysis of the experiments. This research was supported by GATech through the Nanoscience/ Nanoengineering Research Program (NNRP) and the NSF CAREER Grant No. DMR-0349110 (ZD and AM). The work of CZ, RNB, and UL is supported by the DOE and the NSF. Calculations were performed at the Center for Computational Materials Science at Georgia Tech and the National Energy Research Scientific Computing Center (NERSC).

References

[1] U. Landman, W. D. Luedtke, N. A. Burnham, and R. J. Colton, Science **248**, 454 (1990).
[2] U. Landman, Solid State Commun. **107**, 693 (1998).
[3] B. Bhushan, J. N. lsraelachvili, and U. Landman, Nature **374**, 607 (1995).
[4] U. Landman, W. D. Luedtke, and J. Gao, Langmuir **12**, 4514 (1996).
[5] U. Landman, Proc. Natl. Acad. Sci. USA **102**, 6671 (2005).
[6] N. Agraït, A. Levy Yeyati, and J. M. van Ruitenbeek, Phys. Rep. **377**, 81 (2003).

[7] J. I. Pascual, J. Méndez, J. Gómez-Herrero, A. M. Baró, N. Garcia, U. Landman, W. D. Luedtke, E. N. Bogachek, and H.-P. Cheng, Science **267**, 1793 (1995).
[8] U. Landman, W. Luedtke, B. Salisbury, and R. Whetten, Phys. Rev. Lett. **77**, 1362 (1996).
[9] G. Rubio, N. Agraït, and S. Vieira, Phys. Rev. Lett. **76**, 2302 (1996).
[10] E. Scheer, N. Agraït, J. C. Cuevas, A. Levy Yeyati, B. Ludoph, A. Martín-Rodero, G. Rubio Bollinger, J. M. van Ruitenbeek, and C. Urbina, Nature **394**, 154 (1998).
[11] C. J. Muller, J. M. van Ruitenbeek, and L. J. de Jongh, Phys. Rev. Lett. **69**, 140 (1992).
[12] J. I. Pascual, J. Méndez, J. Gómez-Herrero, A. M. Baró, N. García, and Vu Thien Binh, Phys. Rev. Lett. **71**, 1852 (1993).
[13] L. Olesen, E. Laegsgaard, I. Stensgaard, F. Besenbacher, J. Schiotz, P. Stoltze, K. W. Jacobsen, and J. K. Nørskov, Phys. Rev. Lett. **72**, 2251 (1994).
[14] D. P. E. Smith, Science **269**, 371 (1995).
[15] A. Stalder and U. Durig, Appl. Phys. Lett. **68**, 637 (1996).
[16] C. Yannouleas, E. N. Bogachek, and U. Landman, Phys. Rev. B **57**, 4872 (1998).
[17] R. Landauer, IBM J. Res. Dev. **1**, 223 (1957); Phil. Mag. **21**, 863 (1970).
[18] Y. Imry, Introduction to Mesoscopic Physics (Oxford Univ. Press, Oxford, 1997).
[19] E. Bratus', V. Shumeiko, and G. Wendin, Phys. Rev. Lett. **74**, 2110 (1995).
A. Ingerman, G. Johansson, V. S. Shumeiko, and G. Wendin, Phys. Rev. B **64**, 144504 (2001).
[20] E. Scheer, P. Joyez, D. Esteve, C. Urbina, and M. H. Devoret, Phys. Rev. Lett. **78**, 3535 (1997).
[21] B. Ludoph et al., Phys. Rev. B **61**, 8561 (2000).
[22] (a) Z. Dai and A. Marchenkov, Appl. Phys. Lett. **88**, 203120 (2006).
(b) A. Marchenkov, Z. Dai, C. Zhang, R. N. Barnet, and U. Landman, Phys. Rev. Lett. **98**, 046802 (2007).
[23] N. D. Lang, Phys. Rev. B **36**, 8173 (1987).
[24] J. K. Gimzewski, R. Moller, D. W. Pohl, and R. R. Schlittler, Surface Sci. **189/190**, 15 (1987).
[25] D. M. Eigler, C. P. Lutz, and W. E. Rudge, Nature **352**, 600 (1991).
[26] E. N. Bogachek, A. G. Scherbakov, and U. Landman, Phys. Rev. B **53**, R13246 (1996).
[27] K. Terabe, T. Hasegawa, T. Nakayama, and M. Aono, Nature **433**, 47 (2005).
[28] H. Ohnishi, Y. Kondo, and K. Takayanagi, Nature **395**, 780 (1998).
[29] H. Hakkinen, R. N. Barnett, A. G. Scherbakov, and U. Landman, J. Phys. Chem. B **104**, 9063 (2000).
[30] A. I. Yanson, G. Rubio Bollinger, H. E. van der Brom, N. Agraït, and J. M. van Ruitenbeek, Nature **395**, 783 (1998).
[31] V. Rodrigues and D. Ugarte, Phys. Rev. B **63**, 073405 (2001).
[32] H. van den Brom, A. I. Yanson, and J. M. van Ruitenbeek, Physica B **252**, 69 (1998).
[33] J. Taylor, H. Guo, and J. Wang, Phys. Rev. B **63**, 245407 (2001).
[34] M. Brandbyge, J.-L. Mozos, P. Ordejon, J. Taylor, and K. Stokbro, Phys. Rev. B **65**, 165401 (2002).
[35] J. Halbritter, J. Appl. Phys. **97**, 083904 (2005).
[36] R. N. Barnett and U. Landman, Phys. Rev. B **48**, 2081 (1993).
[37] C. Zhang and U. Landman, to be published.
[38] J. P. Perdew, K. Burke, and M. Ernzerhof, Phys. Rev. Lett. **77**, 3865 (1996).
[39] N. Troullier and J. L. Martins, Phys. Rev. B **43**, 1993 (1991).
[40] H. Grönbeck, A. Rosén, and W. Andreoni, Phys. Rev. A **58**, 4630 (1998).
[41] E. Scheer, J. C. Cuevas, A. Levy Yeyati, A. Martín-Rodero, P. Joyez, M. H. Devoret, D. Esteve, and C. Urbina, Physica B **280**, 425 (2000).
[42] M. B. Weissman, Rev. Mod. Phys. **60**, 537 (1988).
[43] A. Halbritter, L. Borda, and A. Zawadowski, Adv. Phys. **53**, 939 (2004).
[44] A similar configuration but with one of the electrodes rotated about the *z*-axis has been used in a self-consistent tight-binding NEGF calculation yielding a conductance of $\sim 2.9G_0$, see J. C. Cuevas, A. Levy Yeyati, and A. Martin-Rodero, Phys. Rev. Lett. **80**, 1066 (1998).
[45] M. Brandbyge, M. R. Sørensen, and K. W. Jacobsen, Phys. Rev. B **56**, 14956 (1997).

